Astronomy Letters, vol. 32, No.6, 2006, pp.361-375 February 5, 2008
Translated from Pis'ma v Astronomicheskii Zhurnal, vol.32, No.6, 2006, pp. 403-418

Structure and Kinematics of the Interstellar Medium in the Star-Forming Region in the BCD Galaxy VII Zw 403 (UGC 6456)

T.A. Lozinskaya[1], A.V. Moiseev[2], V.Yu. Avdeev[1], and O.V. Egorov[1]

[1] Sternberg Astronomical Institute, Universitetskii pr. 13, Moscow, 119992 Russia
[2] Special Astrophysical Observatory, RAS, Nizhnii Arkhyz, Karachai-Cherkessian Republic, 357147 Russia

Abstract. The structure and kinematics of ionized gas in the star-forming region in the BCD galaxy VII Zw 403 (UGC 6456) are analyzed using observations with the SCORPIO focal reducer on the 6-m Special Astrophysical Observatory telescope in three modes: direct imaging (in the Hα, [OIII], and [SII] lines), long-slit spectroscopy, and spectroscopy with a scanning Fabry-Perot interferometer. In addition to the previously known bright HII regions and the faint giant ring that surrounds the entire star-forming region, many new faint diffuse and arc structures have been detected. Fine structure of the giant ring has been revealed. We do not confirm the previously detected expansion of the bright shells around young stellar associations with a velocity of $50 - 70\,\mathrm{km\,s^{-1}}$. We have estimated their expansion velocities to be no higher than 15–20 $\mathrm{km\,s^{-1}}$; the corresponding kinematic age, no younger than 3–4 Myr, agrees well with the age of the compact OB associations related to them. We associate the faint extended filamentary and diffuse regions of ionized gas identified in nearly the entire central region of the galaxy and the giant HII ring with the older (10 Myr) stellar population of the most recent starburst. Weak high-velocity [OIII] and Hα line wings (up to $300\,\mathrm{km\,s^{-1}}$ from the line center) have been detected in the brightest HII region. Such velocities have been observed in the galaxy for the first time. The previously published Hα luminosity measurements for the galaxy are refined.

1. Introduction

Observations of giant shells and supershells around star clusters of various ages in Irr and BCD galaxies provide a unique opportunity to study the interstellar medium in star-forming regions at various epochs. Numerous observations of several nearby galaxies suggest that episodes of violent star formation in galaxies are localized in space and in time and manifest themselves as giant complexes where the bulk of the young stellar population, bright HII regions, and shells and supershells of various scales are concentrated. The "local" interaction of individual OB associations with the ambient interstellar gas shows up most clearly in such complexes.

In this paper, we analyze in detail the structure and kinematics of the shells and supershells that represent traces of several sites of the most recent star formation episode in the BCD galaxy VII Zw 403 (UGC 6456). This is a nearby, isolated, and slowly rotating galaxy that has been studied extensively in the optical, infrared, and X-ray. A study of the stellar population of VII Zw 403 with the Hubble Space Telescope (HST) allowed Lynds et al. (1998) to perform multicolor photometry of individual stars and to reveal several star formation episodes of various intensities in the galaxy. According to these authors, the strongest starburst occurred 800–600 Myr ago. Stars of this generation dominate in the galaxy. Therefore, were it not for the most recent (4–10 Myr ago), relatively weak starburst in the central ~ 1 kpc, the galaxy would be classified as a dwarf elliptical (dE). Loose and Thuan (1985) classified VII Zw 403 as belonging to the most numerous class of BCD galaxies, iE, which is characterized by an irregular bright star-forming region near the center of an extended elliptical halo of old stars. Near-infrared photometry for the stellar population of VII Zw 403 confirms that the region of current star formation is surrounded by an extended "old" stellar halo (Schulte-Ladbeck et al. 1999a).

The star-forming region is observed toward a giant cloud of neutral hydrogen with the highest HI column density in the galaxy and is surrounded by an extended HI halo $3\farcm6 \times 2\farcm9$ or 4.7×3.8 kpc in size (Thuan et al. 2004). The youngest and most massive stars form the distinct associations nos. 1, 2, 3, 4, 5, 6 (for uniformity, we will use the designations from Lynds et al. (1998)). The more evolved stars, including the most luminous red supergiants, are distributed in a more extended region and show no concentration to young clusters. All of the ionized-gas emission is also concentrated in the central region of the galaxy and reveals traces of several sites of the

Send offprint requests to: T.A. Lozinsksaya, e-mail: lozinsk@sai.msu.ru

most recent star formation episode: eight bright HII regions associated with young stellar associations and weak diffuse emission surrounding them (Thuan et al. 1987). Based on HST observations, Lynds et al. (1998) identified a shell structure of several bright HII regions 70–150 pc in size. Silich et al. (2002) found traces of the faint giant ($D \simeq 500$ pc) ring in the Hα emission from the diffuse gas. An extended region of diffuse X-ray emission inside the giant ring was reported, but these data have not yet been confirmed (Papaderos et al. 1994; Lira et al. 2000; Bomans 2001). This question remains open: the observations by Ott et al. (2005a, 2005b) allowed only an upper limit for the diffuse X-ray luminosity to be estimated, $L_X \leq 2.8 \times 10^{38}$ erg s^{-1}.

The results of ionized-gas observations in the galaxy are ambiguous. Thus, for example, the measurements of the total Hα luminosity of the galaxy, which is used as the main criterion for the star formation rate, differ in the papers of Lynds et al. (1998) and Silich et al. (2002) by more than a factor of 20. Based on long-slit spectra taken with the 4-m KPNO telescope, Lynds et al. (1998) found an expansion of bright shells with a velocity $V_{exp} = 50 - 70\,\mathrm{km\,s^{-1}}$, but the observations by Thuan et al. (1987) and Martin (1998) with a higher spectral resolution revealed no such high velocities in the galaxy. All of these factors suggest that further observations of the ionized gas in the star-forming region are required.

We observed the galaxy on the 6-m Special Astrophysical Observatory (SAO) telescope with the SCORPIO focal reducer in three modes: direct imaging in medium-band filters, long-slit spectroscopy, and spectroscopy with a scanning Fabry–Perot interferometer. We will use our observations of the galaxy with the integral field spectrograph MPFS to analyze in detail the gas emission spectrum in our next paper (Lozinskaya et al. 2007). In this paper, we analyze the structure and kinematics of the ionized gas in the star-forming region. In the Introduction, basic data on the galaxy are gathered and the goals of our studies are formulated. Next, the observations and data reduction techniques are described, and the results obtained are presented and discussed. In the final section, we summarize our main conclusions.

In this paper, we assumed the distance to the galaxy to be $d = 4.5$ Mpc (Lynds et al. 1998; Schulte-Ladbeck et al. 1999b), which corresponds to an angular scale of 22 pc arcsec^{-1}.

2. Observations and data reduction

2.1. Interferometric Observations

We performed our interferometric observations of VII Zw 403 on November 30, 2002, at the prime focus of the 6-m SAO telescope (BTA) using the SCORPIO focal reducer; the equivalent focal ratio of the system was $F/2.9$. A description of SCORPIO was given by Afanasiev and Moiseev (2005) and on the Internet (`http://www.sao.ru/hq/lsfvo`); the SCOPRIO capabilities in interferometric observations were also described by Moiseev (2002).

The seeing during the observations varied within the range $1\farcs5 - 2\farcs1$. We used a scanning Fabry-Perot interferometer (FPI) operating in the 501st order at the Hα wavelength. The spacing between the neighboring orders of interference, $\Delta\lambda = 13$ Å, corresponded to a region free from order overlapping with a size of $\sim 600\,\mathrm{km\,s^{-1}}$ on the radial velocity scale. The width of the FPI instrumental profile was ~ 0.8 Å, or $\sim 35\,\mathrm{km\,s^{-1}}$. Premonochromatization was performed using an interference filter with the FWHM $\Delta\lambda = 15$ Å centered on the Hα line. The detector was a TK1024 1024×1024-pixel CCD array. The observations were performed with 2×2-pixel binning to reduce the readout time. In each spectral channel, we obtained 512×512-pixel images at a scale of $0.55''$ per pixel; the total field of view was $4\farcm8$. We took a total of 36 interferograms for various FPI place spacings, so the size of the spectral channel corresponded to $\delta\lambda = 0.36$ Å, or $17\,\mathrm{km\,s^{-1}}$ near Hα. The exposure time was 300 s.

We reduced the raw data using software running in the IDL environment (Moiseev 2002). After the primary reduction, the observational data were represented as a $512 \times 512 \times 36$ data cube; here, a 36-channel spectrum corresponds to each pixel. The final angular resolution (after smoothing during the data reduction) was $\sim 2\farcs2$. The smoothing was performed using the ADHOC software package [1].

We constructed the radial velocity fields and the Hα intensity and FWHM maps using single-component Gaussian fitting of the emission line profile in the data cube. The FWHM map was corrected for the instrumental profile using the "standard" relation (the square root of the difference between the squares of the FWHMs). The formal accuracy of our radial velocity measurements for symmetric line profiles was $\sim 3 - 5\,\mathrm{km\,s^{-1}}$.

All of the radial velocities in this paper are heliocentric.

2.2. Images in Emission Lines

Emission-line and continuum images of VII Zw 403 were obtained on the 6-m SAO telescope with the SCORPIO focal reducer. A log of photometric observations is given in Table 1, which lists the dates of observations, the central wavelengths (λ_c) and full widths at half maximum (FWHMs) of the filters used, the total exposure times T_{exp}, and the average seeing. This table lists the filters whose passbands included the Hα, (Hα+[NII] λ6548, 6583 Å), [OIII] λ4959, 5007 Å, [SII] λ6717 Å lines and the filters centered on the continuum near these lines.

Note that the observations in 2002 were performed with a narrow-band filter centered on the Hα line of the galaxy (this filter was also used for the FPI observations), while the deeper 2003 image was obtained through a fil-

[1] The ADHOC software package was developed by J. Boulestex (Marseilles Observatory).

Table 1. Log of photometric observations

Range	Date	λ_c, Å	FWHM, Å	T_{exp}, s	Seeing
Hα	Nov. 29/30, 2002	6560	15	600	1.″2
Hα continuum	Nov. 29/30, 2002	6608	15	240	1.″2
Hα + [NII]	May 25/26, 2003	6552	75	3000	1.″4
Hα continuum	May 25/26, 2003	6608	15	1500	1.″5
[OIII]	July 23/24, 2003	4995	220	3600	1.″8
[OIII] continuum	July 23/24, 2003	5310	170	1800	1.″8
[SII]	July 22/23, 2003	6720	15	3000	1.″9
[SII] continuum	July 23/24, 2003	6604	21	1200	1.″6

ter whose passband, in addition to Hα, included the two neighboring [NII] lines.

In 2002 and 2003, the detectors were, respectively, a TK1024 CCD array with a scale of 0.28″ per pixel and an EEV42–40 CCD array with a scale of 0.31″ per pixel (in 2×2 readout mode). The data were reduced using a standard procedure; the spectrophotometric standard stars AGK+81 266 and Grw+70 5824 were observed on the same night and almost at the same zenith distance to calibrate the images on the energy scale.

When constructing the maps of "pure" line emission, we subtracted the images in the corresponding continuum from the images in the filters containing the emission lines. In the subtraction, the normalization factor was chosen in such a way that the images of field stars were mutually subtracted in the resulting frame. Since VII Zw 403 is a galaxy with a blue continuum (at any rate in the star-forming region) and since the field stars are mostly red, this (generally accepted) procedure could lead to an underestimation of the contribution from the real continuum for the [OIII] and Hα lines (here, we took a redder filter for the continuum) and, conversely, to an overestimation of the contribution from the continuum for the [SII] images. This effect is very difficult to properly take into account (we do not know the slope of the spectral continuum in different regions of the galaxy and in field stars), which should be remembered when considering the line-ratio maps. For an additional check, we used preliminary spectrophotometric MPFS data for the central region of the galaxy, since the continuum in these observations was subtracted without problems. Unfortunately, our MPFS data are available only for the central region of the galaxy.

2.3. Long-Slit Spectroscopy

Spectral observations of VII Zw403 were performed with the same SCORPIO instrument operating in the mode of a slit spectrograph with a slit about 6′ in length and 1″ in width. The scale along the slit was 0.36″ per pixel. We used volume phase holographic gratings (VPHGs) that provided a spectral resolution of $130 - 140\,\mathrm{km\,s^{-1}}$ near the [OIII] and Hα lines. Since the main objective of the observations with a slit spectrograph was to verify the splitting of the Hβ emission line in bright shells detected by Lynds et al. (1998), we took two spectra with a similar slit localization: scan 1 through regions N2, N3, N4 and scan 2 through the HII regions N1 and N5 (in the designations of Lynds et al. 1998). The position angle of the spectrograph slit was 88° in both cases. In addition to the exposure time T_{exp} and the average seeing, the log of observations (Table 2) also contains the spectral range $\Delta\lambda$.

Table 2. Log of spectral observations

Scan	Date	$\Delta\lambda$, Å	T_{exp}, s	Seeing
1	21/22.12.03	6270–7300	1200	2.″2
1	05/06.12.04	4800–5600	1200	2.0
2	21/22.12.03	6270–7300	1800	2.2
2	05/06.12.04	4800–5600	800	2.0

We took the spectra not only in the "green" spectral range containing the Hβ and [OIII] λ4959, 5007 Å lines, as in Lynds et al. (1998), but also in the "red" spectral range including the Hα, [NII] λ6548, 6583 Å, and [SII] λ6717, 6731 Å lines. The data were reduced in a standard way; the spectrophotometric standard AGK+81 266 observed immediately after the object at a close zenith distance was used for energy calibration.

The radial velocities and FWHMs of the emission lines were determined by single-component Gaussian fitting of their profiles; the observed line FWHMs were corrected for the instrumental profile, as in the case of the FPI data. The accuracy of the absolute velocity measurements was checked using night-sky lines and was $\sim 5\,\mathrm{km\,s^{-1}}$.

3. Results

3.1. General Structure of the Star-Forming Region in the Galaxy

Direct medium-band images of the central region of the galaxy in the (Hα + [NII]), [SII] 6717Å, and [OIII] 5007Å lines were obtained with the SCORPIO focal reducer of the 6-m SAO telescope.

Figure 1 shows the BTA Hα images of the star-forming region on linear and logarithmic scales and its image in a filter containing the Hα line from the HST archive. The numbers in Fig. 1b mark the HII regions identified by Lynds et al. (1998).

As follows from this figure, all of the HII shells N1–N6 identified with HST are seen as the brightest emission re-

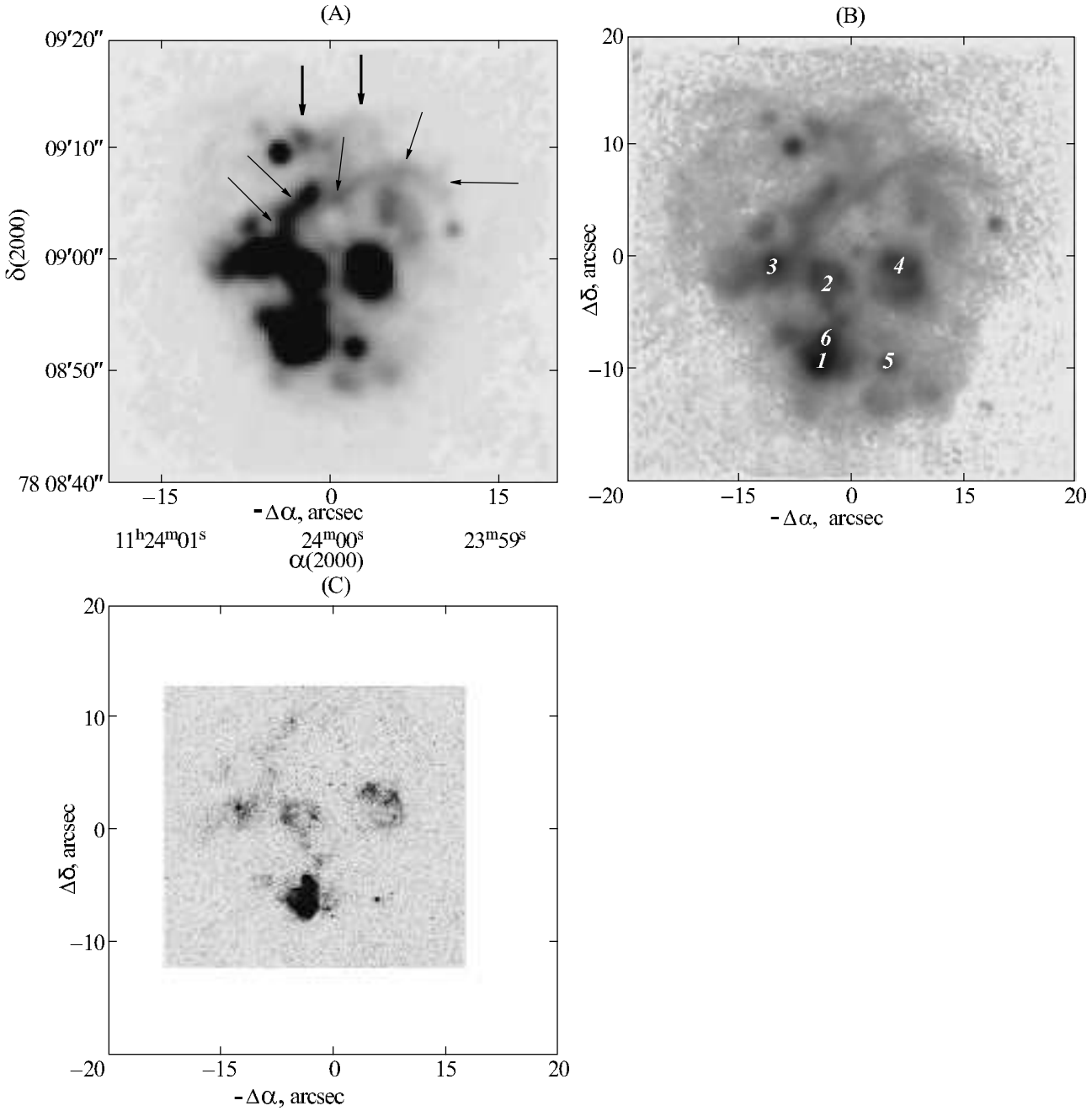

Fig. 1. Hα images of the star-forming region: the images with the SCORPIO focal reducer of the 6-m SAO telescope on (a) linear and (b) logarithmic scales and (c) the WFPC2 image from the HST archive in the F656N filter. The thin arrows indicate the individual arcs which the giant ring identified by Silich et al. (2002) consists of; the thick arrows indicate the outer arc outside this ring. The numbers mark the HII regions identified by Lynds et al. (1998).

gions in our images (with a lower angular resolution that does not allow their shell structure to be revealed). In addition to these previously known bright HII regions, our images reveal a large number of new, fainter emission features. These include spherically symmetric regions ($2-5''$ in size), extended arc and linear structures, and a large region of weak diffuse emission.

Our observations show that the giant shell structure 250 pc in radius torn in the southwest (below referred to as the giant ring) that was identified by Silich et al. (2002) consists of several individual arc structures with different brightnesses and different radii of curvature (see Fig. 1a). Another outer arc and three HII regions about $2''$ in size can be identified in the north outside it.

Figure 2 allows the large-scale structures of the central star-forming region in different lines to be compared. It shows the [OIII] and [SII] images on a logarithmic scale with the Hα+[NII] line contours superimposed and the [OIII]/(Hα+[NII]) and [SII]/(Hα+[NII]) line ratio maps with the same contours superimposed.

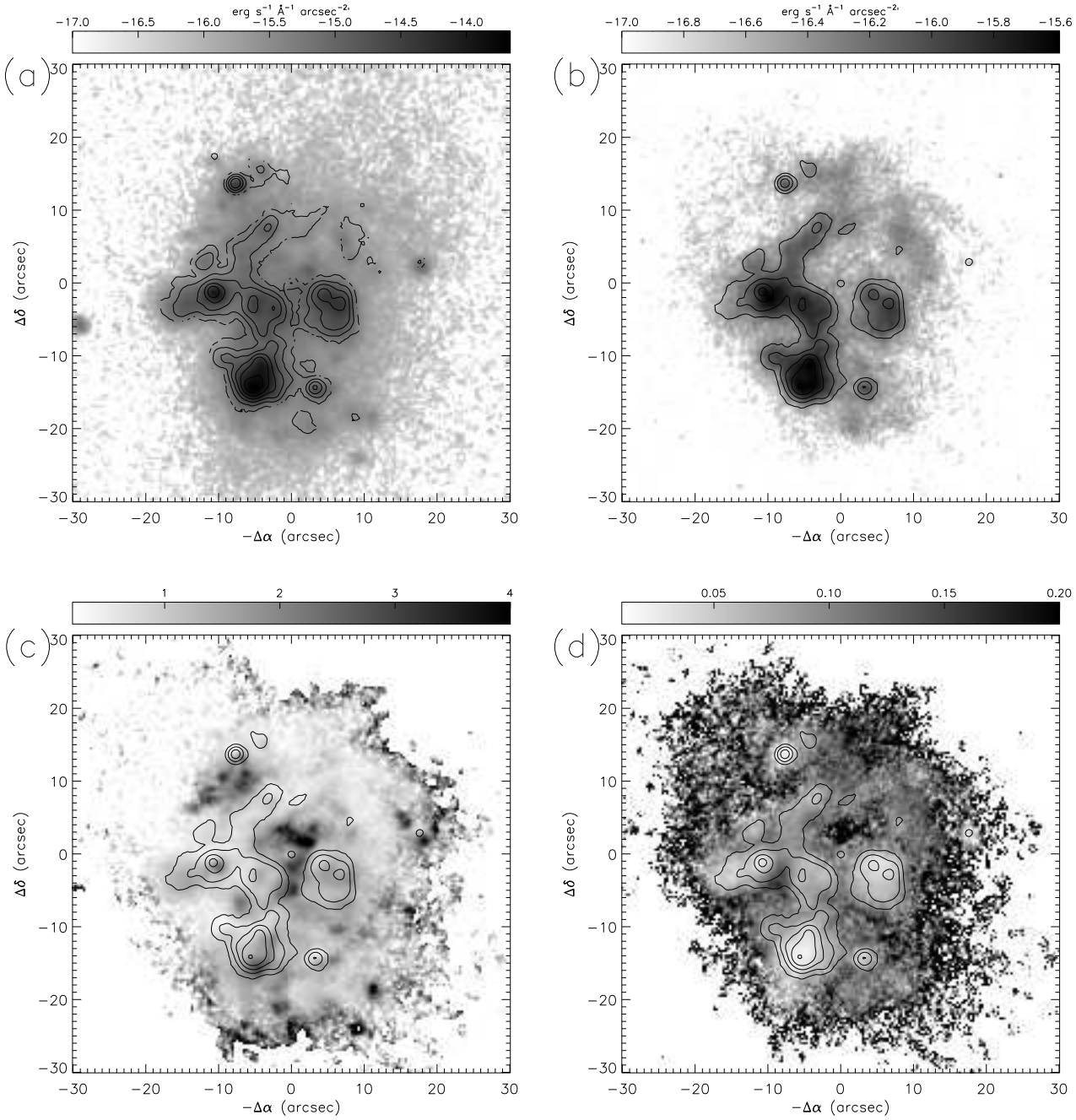

Fig. 2. (a) [OIII] and (b) [SII] images of the star-forming region on a logarithmic scale with the Hα+[NII] line contours superimposed and the (c) [OIII]/(Hα+[NII]) and (d) [SII]/(Hα+[NII]) ratio maps with the same contours superimposed.

As follows from Figs. 1 and 2, in general, the large-scale structures of the star-forming region in the (Hα+ [NII]), [SII], and [OIII] lines are almost identical. Nevertheless, two extended faint regions of diffuse emission in which the [OIII]/(Hα+[NII]) intensity ratio is enhanced can be distinguished. One of these regions lies inside the giant ring between the bright regions N2 and N4 to the north of them, while the second region lies outside the giant ring between it and the outer arc in the north (see Fig. 2c).

The [SII]/(Hα+[NII]) intensity ratio is also enhanced in the first region (see Fig. 2d).

The total size of the region of diffuse ionized gas in the galaxy with all of the bright HII regions observed on its background is $35 - 40''$ or ~ 900 pc at a brightness level of 5×10^{-17} erg s^{-1} cm^{-2} arcsec^{-2}.

We estimated the total Hα flux from the central region of VII Zw 403 by integration within a circular aperture $40''$ in diameter. The fluxes and the corresponding luminosity of the galaxy are given in Table 3. The cor-

Table 3. Estimates of the Hα flux and luminosity for VII Zw 403

Reference	Flux, erg s^{-1} cm^{-2}	L, erg s^{-1}, $D = 4.5$ Mpc
Lynds et al. (1998)	–	1.80×10^{39} (H$_\alpha$)
Martin (1998)	6.5×10^{-13}	1.58×10^{39} (H$_\alpha$ +[NII])
Silich et al. (2002)	1.95×10^{-11}	4.70×10^{40} (H$_\alpha$)
BTA (15A filter)	6.14×10^{-13}	1.49×10^{39} (H$_\alpha$)
BTA (75A filter)	7.96×10^{-13}	1.93×10^{39} (H$_\alpha$ +[NII])

rection for extinction was made for the mean value of $E(B-V) = 0.04$ (and $R_v = A_v/E(B-V) = 3.1$) found by Lynds et al. (1998) from all stars of the galaxy. We corrected the data from Martin (1998) in the same way; the luminosity is given for a distance of 4.5 kpc. Silich et al. (2002) applied a correction only for the background extinction $E(B-V) = 0.02$, as inferred by Burstein and Heiles (1984); the correction for internal extinction in VII Zw 403 increases further the flux and luminosity found by these authors.

As follows from Table 3, our measured Hα luminosity of the galaxy is considerably lower than the value obtained by Silich et al. (2002) and agrees well with the previous estimates by Lynds et al. (1998) and Martin (1998).

3.2. Gas Kinematics in the Star-Forming Region

3.2.1. FPI observations

Based on the observations with FPI, we constructed the Hα radial velocity and FWHM distributions in the central region of the galaxy (see Fig. 3).

The derived velocity of the line peak in the star-forming region ranges from -120 to $-90\,\mathrm{km\,s^{-1}}$ (reaching $-130...-140\,\mathrm{km\,s^{-1}}$ in the region of weak emission at the edge of the field). These velocities agree well with the neutral-gas velocity from -120 to $-80\,\mathrm{km\,s^{-1}}$ in the extended surrounding region of the galaxy and from -110 to $-90\,\mathrm{km\,s^{-1}}$ in the densest HI cloud in the galaxy with which the star-forming region coincides (Thuan et al. 2004).

The Hα FWHM corrected for the instrumental profile lies within the range $60-70$ to $100-120\,\mathrm{km\,s^{-1}}$.

To find the expansion of the bright spherically symmetric HII regions, we constructed the so-called position–velocity (P/V) and position–FWHM ($P/\Delta V$) diagrams. The orientation of the scans was chosen in such a way that they crossed in two or three different directions each of the HII regions, including those that reveal a well-defined shell structure in the HST images (the HII regions N1, N3, and N4) and whose expansion with velocities of $50-70\,\mathrm{km\,s^{-1}}$ was reported by Lynds et al. (1998).

As an example, Fig. 4 shows four of more than thirty our scans.

The most extended shell N4 $6.5-8''$ (140–180 pc) in size showed an increase in the line FWHM toward the center to $\Delta V = 90\,\mathrm{km\,s^{-1}}$ compared to $\Delta V = 65-70\,\mathrm{km\,s^{-1}}$ in the bright northern and southern peripheral parts. This may be the result of its expansion with a velocity of $15-20\,\mathrm{km\,s^{-1}}$ (see scan 4 in Fig. 4).

According to our FPI observations, none of the bright HII regions, except N4, revealed the velocity-ellipse structure characteristic of an expanding thin shell in the P/V diagrams or line broadening at the center in the $P/\Delta V$ diagrams.

In the region of the richest OB association and the brightest HII shell N1, the HST image shows a chain of associations and HII regions associated with them: supershell N1 (around association no. 1), the HII region N6 (around association no. 3), and another region associated with association no. 2 between them. (To avoid confusion , we retained all of the designations from Lynds et al. (1998)). Scan 1 in Fig. 4 passes along this chain; our observations revealed no changes in the line velocity or FWHM in this chain of HII regions.

The line FWHM in the bright shells showing no evidence of expansion is $60\,\mathrm{km\,s^{-1}}$, which exceeds the contribution from the thermal and turbulent velocities in HII regions. Of course, at an angular resolution of $2\farcs2$, we average all of the radial velocity variations over a region comparable in radius to the shell. However, in any case, the hypothetical expansion velocity of these shells that could explain the observed line FWHM does not exceed $15-20\,\mathrm{km\,s^{-1}}$.

Based on the FPI observations, we determined the mean line velocities and FWHMs in all of the faint Hα emission regions that were first identified in our images. No appreciable line velocity and FWHM variations indicative of expansion with a velocity higher than $20\,\mathrm{km\,s^{-1}}$ were found in any of them either.

To summarize the results of our kinematic studies with FPI, we conclude that no sharp variations of the Hα velocity and FWHM are observed in the entire star-forming region on scales larger than 45–50 pc, which corresponds to the actual angular resolution of $2\farcs2$ for our FPI observations. The observed velocity variations lie within the range $\pm(10-20)\,\mathrm{km\,s^{-1}}$; the line FWHM ranges from 60 to $100-120\,\mathrm{km\,s^{-1}}$.

The accuracy of our measurements is high enough for the fast shell expansion reported by Lynds et al. (1998) to be detected. Thus, for example, the constructed FPI maps clearly show a relationship between the HII regions and the variations in the radial velocities and velocity dispersion of the gaseous clouds (line FWHM).

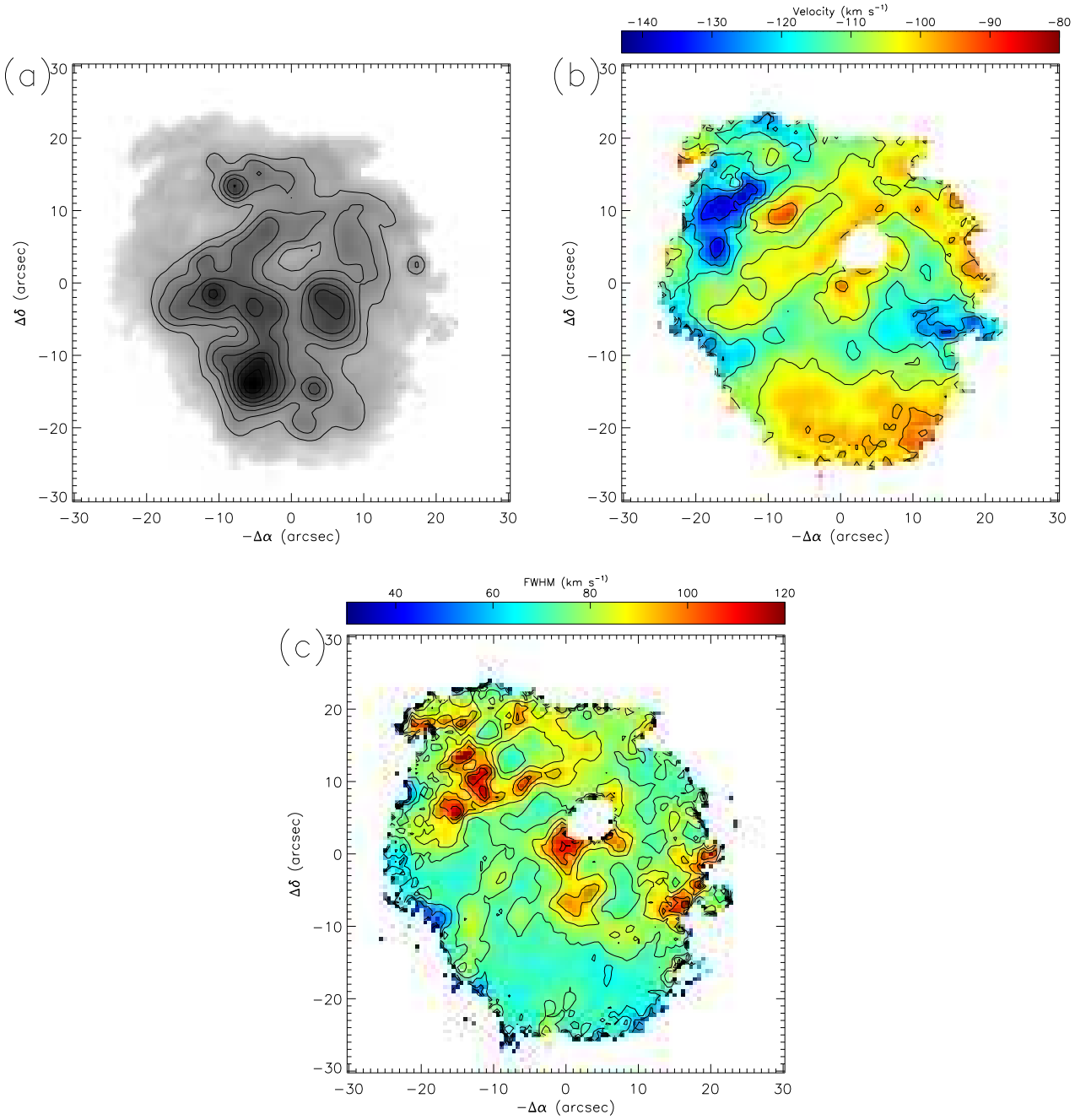

Fig. 3. Hα intensity (a), radial velocity (b), and FWHM (c) distributions constructed from the FPI observations. The "hole" in the central region results from a parasitic ghost inside the instrument.

3.2.2. Long-slit spectroscopy

To elucidate the cause of the discrepancies in the expansion velocities of the bright shells estimated from the spectral observations by Lynds et al. (1998) and from our FPI observations, we performed long-slit spectroscopy in the red (Hα, [NII], [SII]) and green (Hβ, [OIII]) spectral ranges. The spectral observations were performed under the conditions closest to those in the observations by Lynds et al. (1998). The actual spectral resolution (estimated from sky lines) was FWHM=120 km s^{-1}, which is comparable to that in the above work. The angular resolution was also similar, 2″; it was limited by seeing in our work and equal to the spectrograph slit width in Lynds et al (1998).

In both ranges, we made two scans through the same regions of the shells whose spectra are presented in Lynds et al. (1998). The spectrograph slit localization is shown in Fig. 4a.

Figure 5 shows the Hα and [OIII] lines in each of the two scans at different intensity levels and Gaussian fits of their profiles.

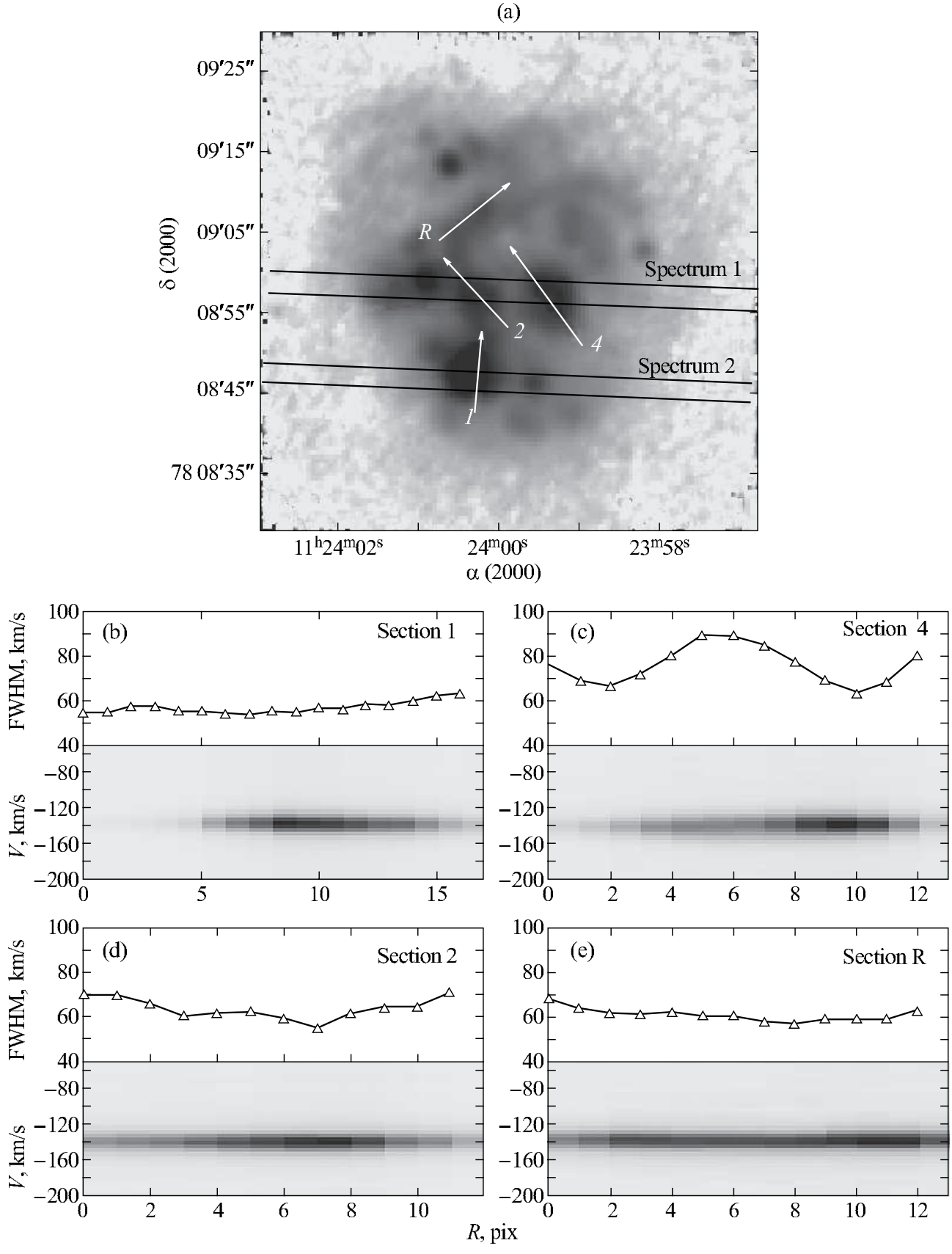

Fig. 4. (a) Orientation of the scans chosen as an example together with the spectrograph slit localization for the two spectra obtained. (b)–(e) Examples of the position–velocity (P/V) and position–FWHM ($P/\Delta V$) diagrams constructed from the FPI observations.

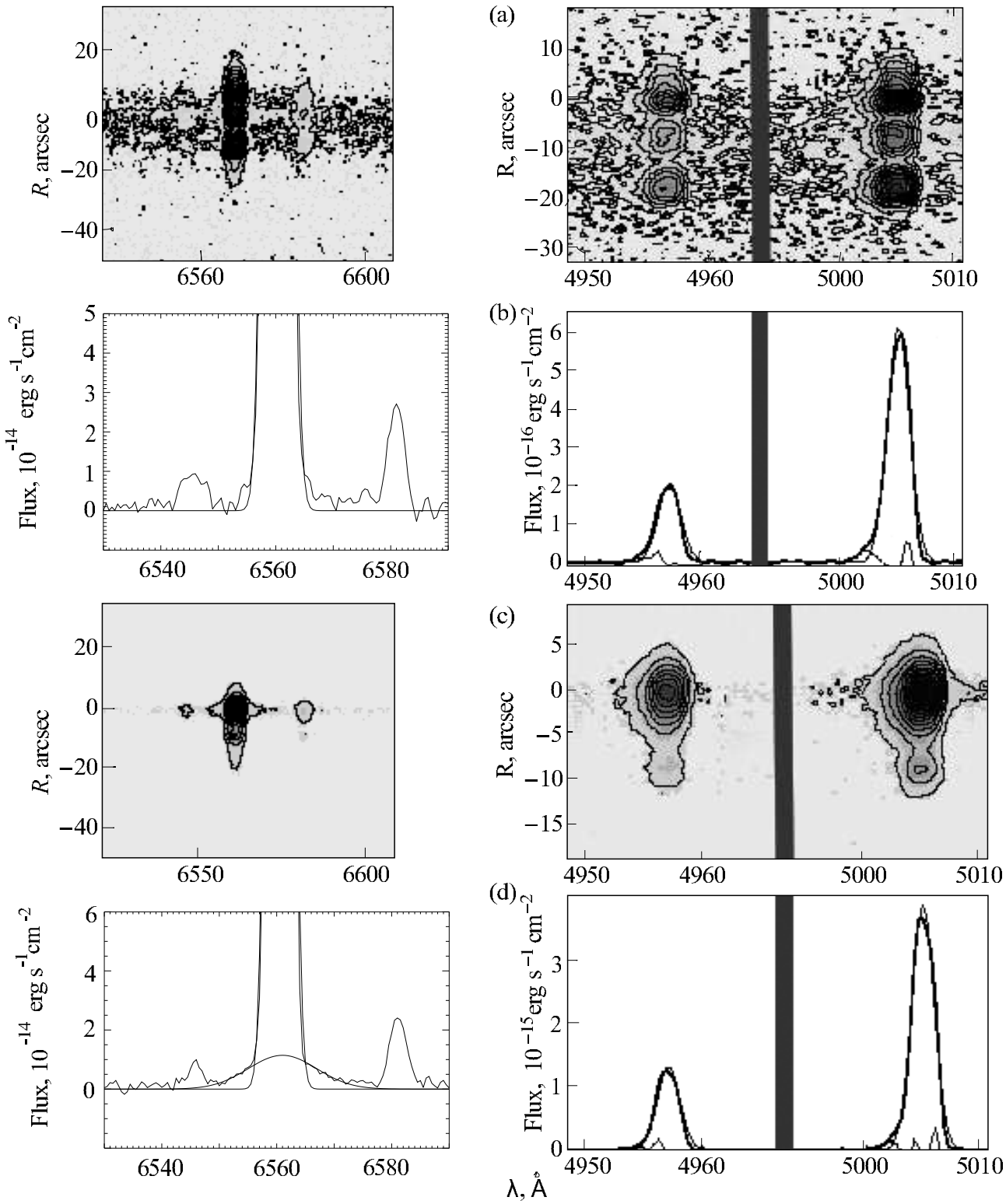

Fig. 5. Spectra around Hα (on the left) and [OIII] (on the right) lines at various intensity levels and their Gaussian fits for two spectra: (a, b) spectrum 1 and (c, d) spectrum 2. The localization of the spectrograph's slits is shown in Fig. 4a.

No distinct profile splitting that would be indicative of the expansion of the ionized supershells with a velocity of $50-70\,\mathrm{km\,s^{-1}}$ was found in any of the lines in the spectra. A single-component Gaussian fits well the profiles of the Hβ, Hα, and forbidden lines in the bright supershells N2, N3, N4, and N5; the residuals are small.

Very weak high-velocity [OIII] and Hα line wings are observed in the brightest shell N1 around the richest and

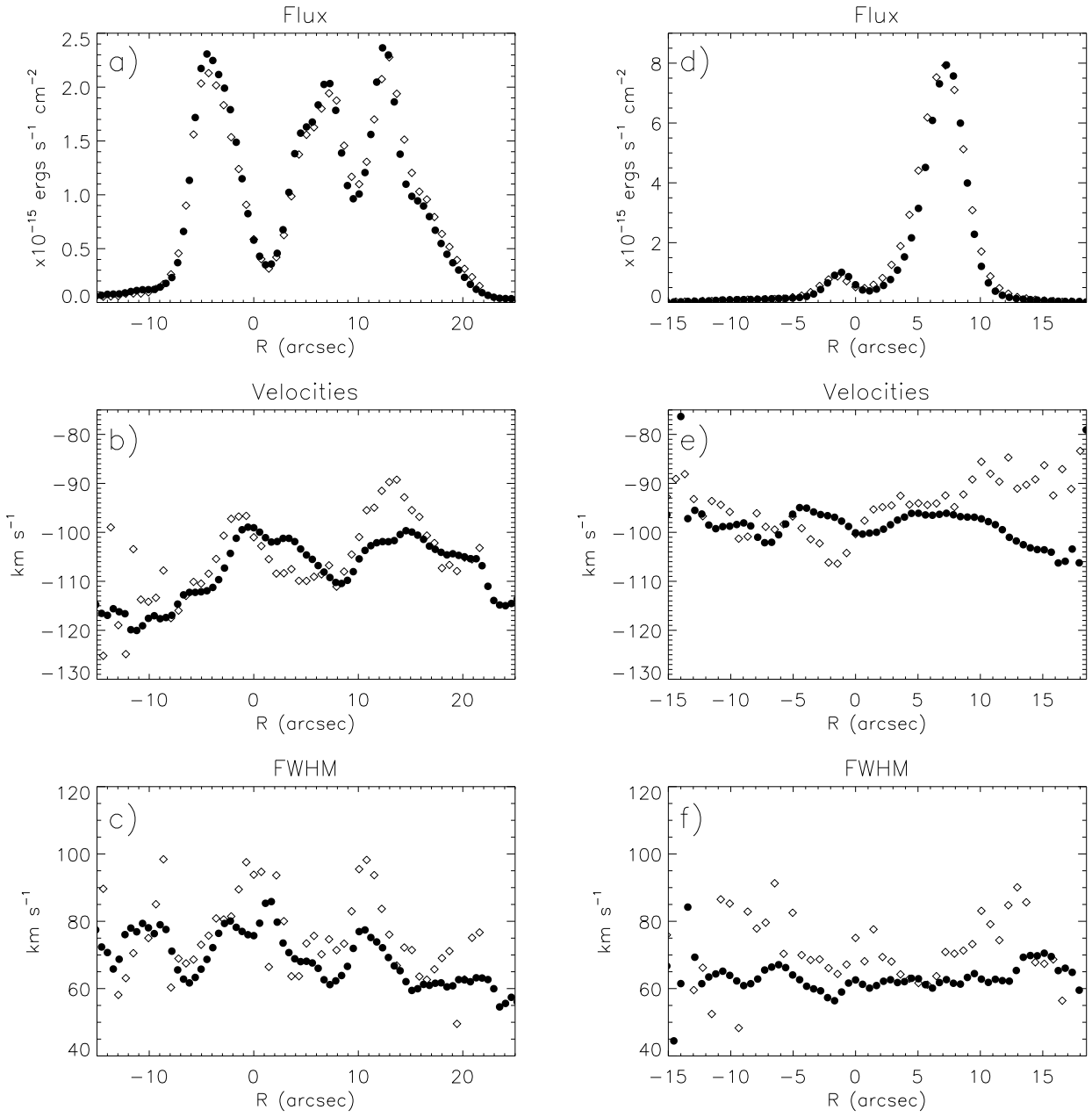

Fig. 6. Comparison of the results of our spectral (open diamonds) and interferometric (black circles) observations: Hα intensity, radial velocity, and FWHM variations along the two scans corresponding to the spectrograph slit position shown in Fig. 4a: (a, b, c) spectrum 1 and (d, e, f) spectrum 2.

youngest association no. 1. As we see from Figs. 5c and 5d, the [OIII] line here is asymmetric and reveals a weak blue component with velocities of $-200..-300\,\mathrm{km\,s^{-1}}$ from the line center at $\sim 5\%$ of the maximum. The Hα line exhibits a weak broad pedestal that can be fitted by a Gaussian with FWHM=630 $\mathrm{km\,s^{-1}}$; the total flux in the broad component is $\sim 4\%$ of the total flux in the line.

Such high velocities have been detected in the galaxy for the first time and, in all probability, are indicative of gas acceleration at the shock front. Of course, given the very low intensity of the high-velocity features, these results must be confirmed by independent observations. We performed several tests to check whether these spectral features are instrumental effects (a complex structure of the instrumental contour of the spectrograph, focusing peculiarities, etc.). In particular, we checked the shape of the instrumental profile using both intense sky lines and a calibration comparison spectrum and made sure that the instrumental profile contained no broad wings, at any rate above $0.5-1\%$ of the maximum. Note also that the relative intensity of the broad pedestal exceeds the intensity of the scattered light in the SCORPIO spectrograph with VPHG gratings (according to our estimates, less than 1%).

Figure 6 compares the results of our spectral and interferometric observations: the Hα intensity, radial velocity, and FWHM variations along scans 1 and 2 whose localization is shown in Fig. 4a (spectra 1 and 2).

First of all, this figure is an independent test of the reduction of the data from the two observing programs for correctness: as we see, the agreement between both the radial velocities and the FWHMs of the lines derived from our interferometric and spectral data is satisfactory. As we noted above, no line broadening at the center is seen in the bright HII regions, as was expected for shells expanding with velocities of $50-70\,\mathrm{km\,s^{-1}}$. In contrast, a clear line broadening (from FWHM$\simeq 60-70\,\mathrm{km\,s^{-1}}$ to FWHM $\simeq 80-120\,\mathrm{km\,s^{-1}}$) is observed in the faint region of diffuse ionized gas between the bright HII regions N4 and N2 as well as between regions N3 and N2. This effect is also present in the second scan crossing regions N1 and N5, but it is less prominent.

Our observations in the [OIII] line also revealed a similar line broadening in the region of weak diffuse emission compared to the bright HII regions. Thuan et al. (1987) also pointed out that the bright HII regions are characterized by the median radial velocities, while the minimum and maximum Hα velocities are observed in the weak diffuse emission between them.

The large-scale neutral-gas kinematics in the star-forming region reveals a distinct gradient in the radial velocity of the 21-cm line peak (see Fig. 20 in Thuan et al. 2004). In the direction from northeast to southwest, the velocity smoothly increases from -110 to $-95-$ $-85\,\mathrm{km\,s^{-1}}$ in both HI clouds elongated in this direction. The nature of this gradient is unclear; the above authors suggest that the gas may rotate in the central region along the major axis of the galaxy. We attempted to find the same gradient in the ionized-gas velocity distribution in the region. To this end, we constructed from our FPI Hα observations P/V diagrams in the directions identical to those of the P/V diagrams for HI in Thuan et al. (2004). We found no similar smooth gradient in the Hα radial velocity.

4. Discussion

Our (Hα + [NII]), [SII], and [OIII] images for the central region of the galaxy suggest that the large-scale structures of the star-forming region in these lines are identical. All of the previously identified HII regions are seen as the brightest emission features in our images in all of these lines (see Figs. 1, 2, 4a). In addition, we detected a large number of new, weaker emission features, both compact and extended diffuse, arc, and linear structures. We were able to resolve the giant ring identified by Silich et al. (2002) into several individual arc structures with different brightnesses and different radii of curvature. Another faint outer arc can be distinguished in the north outside the ring. All of the bright emission features are observed on the background of weak diffuse ionized-gas emission.

Our Hα-luminosity estimate for the galaxy is considerably lower than the value obtained by Silich et al. (2002) and agrees well with its previous estimates by Lynds et al. (1998) and Martin (1998).

According to our long-slit spectroscopy presented above and our preliminary data (Lozinskaya et al. 2007), the ([NII]λ6548, 6583)/Hα intensity ratio in VII Zw 403 is $\sim$ 0.03–0.035; a similar value of 0.03 was obtained by Martin (1997). Accordingly, the (Hα + [NII]) luminosity determined from a deeper image with a broad-band filter (see Table 3) gives $L(\mathrm{H}\alpha) = 1.86\times10^{39}$ erg s^{-1}.

Using the formula for estimating the star formation rate (SFR) from the Hα luminosity, SFR ($M_\odot\,\mathrm{yr}^{-1}$) = $7.9\times10^{-42}L(H\alpha)$ (Kennicutt 1998), we obtain SFR = $0.012-0.015M_\odot\mathrm{yr}^{-1}$ from the derived luminosity $L(H\alpha) = (1.49-1.86)\times10^{39}$ erg s^{-1} for the mass range 1 to $100M_\odot$.

Based on our interferometric Hα observations with FPI, we constructed the line radial velocity and FWHM distributions in the central region of the galaxy with an angular resolution of $2\farcs2$. The Hα FWHM in the star-forming region lies within the range 60-70 to $100-120\,\mathrm{km\,s^{-1}}$. The ionized-gas velocity in the star-forming region from -120 to $-90\,\mathrm{km\,s^{-1}}$ agrees well with the neutral-gas velocity in the two dense HI clouds coincident with it that was measured by Thuan et al. (2004).

We failed to detect the expansion of the bright spherically symmetric HII regions with a velocity of $50-70\,\mathrm{km\,s^{-1}}$ that was reported by Lynds et al. (1998). In our opinion, the most likely cause of the difference between the results of Lynds et al. (1998) and our results is that these authors used a slit with a width of $2''$, which is clearly slightly larger than the characteristic seeing at the KPNO Observatory. For a relatively wide slit, the coherent structures resembling the velocity ellipses of rapidly expanding shells in the spectra by Lynds et al. can result from brightness variations in the object across the slit, so that the spatial and spectral features are mixed at the output from the spectrograph. Unfortunately, the above paper contains no seeing data and we cannot test this assumption. Note also that the Hα observations by Thuan et al. (1987) with FPI and the observations by Martin (1998) with an echelle spectrograph with a spectral resolution corresponding to $11\,\mathrm{km\,s^{-1}}$ did not reveal any gas motions with such velocities anywhere in the galaxy either.

We estimated the expansion velocity for shell N4 $6.5-8''$ (140-180 pc) in size from the observed line broadening toward the center to be $15-20\,\mathrm{km\,s^{-1}}$.

The corresponding kinematic age of the shell in the standard model by McCray and Kafatos (1987) is $\sim$ 3–4 Myr. The association no. 5 responsible for the formation of this shell contains 28 blue main-sequence stars and supergiants; the age of the association is 5–6 Myr (Lynds et al. 1998).

We estimated the upper limit for the expansion velocity of the remaining bright HII regions from the Hα, Hβ, and [OIII] FWHMs to be $\mathrm{V_{exp}} \le 15-20\,\mathrm{km\,s^{-1}}$.

The corresponding kinematic age of the shells reaches 3–4 Myr or more. This is considerably closer to the age of the compact associations responsible for their formation than the kinematic age of the shells, ~ 1 Myr, found by Lynds et al. (1998) using the same standard model at the high expansion velocity.

The age of the richest association no. 1 associated with shell N1 was estimated by Lynds et al. (1998) to be 4–5 Myr. Associations nos. 2, 3, 4, and 6 are considerably poorer than associations nos. 1 and 5 and are also identified with the bright compact HII regions: associations nos. 3, 4, and 6 are identified with the HII regions N6, N3, and N5, respectively.

In addition to these relatively compact associations, HST observations also revealed luminous blue stars in the entire central field of the galaxy. A more sparse grouping of stars designated as "center" in Fig. 2 and Fig. 11 from Lynds et al. (1998) was identified at the center of the star-forming region; the fainter diffuse shell N2 200–240 pc in size is associated with it. This mixed-age association contains a group of blue supergiants (~ 5 Myr old) coincident with an older population (no younger than 10 Myr), including 20 red supergiants of this age. Two populations of stars with ages of 5 and 10 Myr or slightly older are also observed in the field designated as "north" and "south" by Lynds et al. (1998).

Thus, the central part of the galaxy reveals two starbursts 5 and 10 Myr ago; the interstellar medium shows traces of these two bursts of the most recent star formation episode. All of the mentioned bright HII regions were identified with the associations formed ~ 5 Myr ago. The fainter filamentary and diffuse Hα emission regions distinguished in the entire central region as well as the giant ring of ionized gas and the outer arc outside it can most likely be associated with the older stellar population whose age reaches 10 Myr.

In general, the detected line broadening in the weak diffuse emission of ionized gas outside the bright HII regions may result from the superposition of several faint background regions of ionized gas along the line of sight located in the gaseous galactic disk and emitting at different radial velocities. However, another possibility is of greater interest: the observed line broadening may be attributable to a more efficient acceleration of the low-density gas by shock waves. The latter assumption can be tested observationally based on the line intensity ratios in the spectrum. As we noted above, the emission in the [OIII] and [SII] lines is actually enhanced with respect to Hα in the region of weak diffuse emission between the bright HII regions N4 and N2 as well as to the north of regions N3 and N2 (see Fig. 2c). The regions of maximum Hα FWHM are also localized approximately here. This part of the star-forming complex coincides with the region of comparatively weak 21-cm line emission between the two densest HI clouds, which also has a higher neutral-gas velocity dispersion than that in the clouds (Thuan et al. 2004). All of these facts may provide evidence for a significant influence of the shock waves generated by stellar wind and supernovae of the older population mentioned above on the low-density gas. The age of 10 Myr suggests that it is in these regions, not in the younger compact associations associated with the bright shells, that the massive stars have already begun to go away from the main sequence and supernova explosions occur in the star-forming region.

The question about the nature of the weak diffuse emission of ionized gas in irregular galaxies has remained open for several decades. The action of shock waves is actually considered as an additional excitation source of forbidden lines. In VII Zw 403, the problem is compounded by the fact that the diffuse emission of ionized gas is anomalously weak in this galaxy. (For this reason, having observed 14 nearest irregular galaxies, Martin (1987, 1988) excluded VII Zw 403 from her analysis when discussing the nature of the diffuse ionized gas.) Given the low intensity of the Hα emission in the two diffuse regions mentioned above, our estimates of the line intensity ratios must be confirmed by MPFS observations. We have already performed MPFS observations; the emission spectrum of the diffuse ionized gas and bright HII regions in the galaxy will be analyzed in detail in our forthcoming paper (Lozinskaya et al. 2007). Here, we only point out a preliminary result: our MPFS observations are consistent with the filter observations presented here.

The very weak high-velocity Hα and [OIII] wings detected in the brightest supershell N1 all the more require confirmation. Such velocities, up to $-200 - -300\,\mathrm{km\,s^{-1}}$ from the [OIII] line center (at $\sim 5\%$ of $I_{\max}$) and the weak broad Hα pedestal corresponding to turbulent velocities with FWHM up to $630\,\mathrm{km\,s^{-1}}$ (i.e., a gas velocity dispersion up to $270\,\mathrm{km\,s^{-1}}$) have been detected in the galaxy VII Zw 403 for the first time. If these results were confirmed by independent observations, such high velocities would unambiguously prove that the gas accelerates at the shock front.

Note that the same two-component kinematics, faint high-velocity features in slowly expanding shells, was observed in several galactic supershells of similar sizes and was explained by the action of a Wolf–Rayet stellar wind and/or by supernovae explosions inside old supershells (see Lozinskaya (1998) and references therein). Weak high-velocity Hα wings are also observed in bright HII regions of other spiral galaxies (see Relaño and Beckman (2005) and references therein). However, in both cases, the velocities are no larger than $100 - 200\,\mathrm{km\,s^{-1}}$ from the line center.

Of greater interest is the detection of a weak broad component in the Hα line with FWHM=$1000\,\mathrm{km\,s^{-1}}$ in the central region of the BCD galaxy SBS 0335–052 (Pramskij and Moiseev 2003). The relative intensity of the broad component accounted for $\sim 2\%$ of the narrow component, i.e., approximately the same as that in our case. Given the lower gas density in dwarf galaxies, the same energy input from supernovae or stellar wind must actually produce shock waves propagating with velocities higher than those in spiral galaxies. As an example, we may note a recent paper by Pustilnik et al. (2004) de-

voted to the BCD galaxy HS 0837+4717, who detected a broad (FWHM=1300 $\mathrm{km\,s^{-1}}$) and higher-contrast (up to 16%) pedestal in the Hα line. The high-velocity component has an unusually large Balmer decrement, which the authors attribute both to electron impact line excitation and to high internal extinction in the formation region of this component.

Another problem that requires further studies is a detailed comparison of the ionized- and neutral-gas kinematics in the central region of VII Zw 403. It seems important for establishing the genetic connection between the star-forming region and the dense HI complex at the center of the galaxy.

5. Conclusions

Thus, our long-slit spectroscopy with the same spectral resolution as the spectral observations by Lynds et al. (1998), and our FPI observations with three times the resolution of Lynds et al. (1998) revealed no evidence of the expansion of the bright shells with velocities of $50-70\,\mathrm{km\,s^{-1}}$.

The expansion velocity of the most extended shell N4 determined from the Hα line broadening in the central region reaches $15-20\,\mathrm{km\,s^{-1}}$. The upper limit for the expansion velocity of the remaining bright HII regions estimated from the Hα, Hβ, and [OIII] line FWHMs does not exceed $15-20\,\mathrm{km\,s^{-1}}$. The corresponding kinematic age of the bright HII shells is 3–4 Myr or more, in close agreement with the age of 4–5 Myr for the compact OB associations associated with them, as estimated by Lynds et al. (1998).

Weak high-velocity wings of the [OIII] line (up to $-200...-300\,\mathrm{km\,s^{-1}}$ from the line center) and Hα line (with FWHM as large as $600\,\mathrm{km\,s^{-1}}$ and a total flux in the broad component reaching 4% of the total intensity) were detected in the brightest shell N1 around the richest and youngest association no. 1. Such velocities have been observed in the galaxy VII Zw 403 for the first time.

We associate the faint filamentary and diffuse emission regions that were identified in nearly the entire central region of the galaxy and the giant ring of ionized gas with the older and more "sparse " stellar population of the most recent starburst whose age was estimated by Lynds et al. (1998) to be 10 Myr.

Our estimate of the total Hα luminosity for the galaxy $L_{\mathrm{H}\alpha} = (1.49-1.86)\times10^{39}$ erg $\mathrm{s^{-1}}$ does not confirm the measurements by Silich et al. (2002), but agrees well with the earlier measurements by Lynds et al. (1998) and Martin (1998).

Acknowledgements. This work was supported by the Russian Foundation for Basic Research (project nos. 04-02-16042 and 05-02-16454). A.V. Moiseev thanks the Foundation for Support of Russian Science for partial support. The work is based on the observational data obtained with the 6-m SAO telescope financed by the Ministry of Science of Russia (registration no. 01-43) and, in part, on the NASA/ESA Hubble Space Telescope data retrieved from the Space Telescope Science Institute archive operated by the Association of Universities for research in astronomy under contract with NASA (NAS 5-26555). We also wish to thank N. Podorvanyuk and M. Yakim for help with the observations on the 6-m SAO telescope.

References

Afanasiev V.L. and Moiseev A.V., 2005, Astron. Lett. **31**, 194 [astro-ph/0502095]

Bomans D., 2001, Rev. Mod. Astron. **14**, 297

Burstein D. and Heiles C., 1984, Astrophys. J., Suppl. Ser. **54**, 33

Kennicutt R.C., 1998. Ann. Rev. Astron. Astrophys. **36**, 189

Lira P., Lawrence A., and Johnson R.A., 2000, Mon. Not. R. Astron. Soc. **319**, 17

Loose H.-H. and Thuan T.X., 1985, *Star-Forming Dwarf Galaxies and Related Objects,* Ed. by D. Kunth, T.X. Thuan (Frontieres, J. Tran Thanh Van Gif-sur-Yvette), 73

Lozinskaya T.A., 1998. Astron. Lett. **24**, 237

Lozinskaya T.A., Moiseev A.V., Avdeev V.Yu., and Egorov O.V., 2007, in preparation

Lynds R., Tolstoy E., O'Neil E.J., and Hunter D.A., Astron. J. **116**, 146

Martin C.L., 1997, Astrophys. J. **491**, 561

Martin C.L., 1998, Astrophys. J. **506**, 222

McCray R. and Kafatos M., 1987, Astrophys. J. **317**, 190

Moiseev A.V., 2002, Bull. Spec. Aastrophys. Obs. **54**, 74 [astro-ph/0211104]

Ott J., Walter F., and Brinks E., 2005a, Mon. Not. R. Astron. Soc. **358**, 1423

Ott J., Walter F., and Brinks E., 2005, Mon. Not. R. Astron. Soc. **358**, 1453

Papaderos P., Fricke K.J., Thuan T.X., and Loose H.-H., 1994, Astron. Astrophys. **291**, L13

Pramskij A.G. and Moiseev A.V., 2003, Preprint N188, SAO RAN (Special Astrophysical Observatory, Russian Academy of Science), 1.

Pustilnik S., Kniazev A., Pramskij A., et al., 2004, Astron. Astrophys. **419**, 469

Relaño M., and Beckman J.E., Astron. Astrophys., 2005, **430**, 911

Schulte-Ladbeck R.E., Hopp U., Greggio L., and Crone M.M., 1999a, Astron. J. **118**, 2705

Schulte-Ladbeck R.E., Hopp U., Crone M.M., and Greggio L., 1999b, Astrophys. J. **525**, 709

Silich S., Tenorio-Tagle G., Muñoz-Tuñón C., and Cairós L.M., 2002, Astron. J. **123**, 2438

Thuan T.X., Hibbard J.E., and Levrier F., 2004, Astron. J. **128**, 717

Thuan T.X., Williams T.B., and Malumuth E., 1987, in *Starburst and Galaxy Evolution. Procedings of the 22-th Moriond Astrophysical Meeting* (Frontieres, Gif-sur-Yvette, 1987), 151.

Translated by V. Astakhov